Journal of
Composites Science

MDPI

Article

Anticorrosion Properties of Epoxy Composite Coating Reinforced by Molybdate-Intercalated Functionalized Layered Double Hydroxide

Suman Chhetri [1,2], Pranab Samanta [1,2], Naresh Chandra Murmu [1,2,*] and Tapas Kuila [1,2,*]

[1] Surface Engineering & Tribology Division, Council of Scientific and Industrial Research-Central Mechanical Engineering Research Institute, Durgapur 713209, India; schhetri79@yahoo.com (S.C.); ps.iitb@gmail.com (P.S.)
[2] Academy of Scientific and Innovative Research (AcSIR), Ghaziabad 201002, India
* Correspondence: ncmurmu@gmail.com (N.C.M.); tkuila@gmail.com (T.K.)

Received: 11 December 2018; Accepted: 10 January 2019; Published: 15 January 2019

Abstract: Herein, an intercalation modification technique is proposed to improve the anticorrosion performance of polymeric coatings. Molybdate, an inhibitor, was intercalated to bestow inhibitive attributes, while functionalization of the layered double hydroxide (LDH) reservoir was performed to augment the interfacial adhesion of LDH with the polymer matrix and steel surfaces. The intercalation and functionalization of Mg–Al–LDH was characterized by Fourier-transform infrared spectroscopy, X-ray diffraction, and thermogravimetric analysis. The corrosion inhibition effectiveness of the prepared composite coating was analyzed using potentiodynamic polarization and electrochemical impedance spectroscopy. The electrochemical results revealed that the protective performance of epoxy coating was significantly enhanced by the addition of functionalized double hydroxide. The corrosion protection efficiency of the composite coating was improved by more than 98%, while the corrosion rate was lowered by ~98%, respectively, with the addition of 1 wt.% of functionalized LDH.

Keywords: intercalation; functionalization; coating; anticorrosion; impedance spectroscopy

1. Introduction

Corrosion-induced premature degradation of metallic infrastructure has been a major concern for industrial growth and prosperity. From the simplest fastener nail to enormous underground pipes, all metallic substrates have the propensity to corrode in the presence of H_2O, O_2, Cl^-, etc. It is not prudent to quantify corrosion only in terms of gross domestic product loss, as it also affects human health and the environment. Although absolute prevention of inevitable corrosion is not feasible, the process can possibly be delayed by applying coatings, using corrosion inhibitors, alloying, etc. [1,2]. Among others, the application of a polymeric coating over the metal substrate has been widely adopted as a protective strategy due to its ease of application, good anticorrosion performance, and low toxicity [3]. A polymeric coating acts as a barrier against the ingress of oxygen, water, and other corrosive ions, obstructing the metal surface from coming into direct contact with corrosive ions. Among polymeric coatings, epoxy resins are mostly used on account of their excellent corrosion resistance, outstanding adhesion properties, low shrinkage, and good mechanical and thermal properties. Despite of its many beneficial attributes, epoxy resins are highly brittle and have poor impact resistance and flexibility, which results in the formation of numerous tiny pores and microcracks due to mechanical damage. Further, prolonged exposure to corrosive ions leads to hydrolytic degradation of the epoxy matrix, which serves as a path for the ingress of corrosive

ions [4,5]. Thus, to improve the durability and longevity of epoxy-based coatings, the inclusion of a nanofiller as a protective barrier or inhibitor is inevitable. The incorporated nanofiller improves the anticorrosion performance of the coating by increasing the diffusion path length of corrosive ions, thus restraining the formation of micropores and cavities. The incorporation of a filler within the epoxy resin addresses the above bottleneck and further augments its anticorrosion properties. In composites, the constituent components retain their intrinsic properties at the microscale level, but at macroscopic level, the composites exhibit properties superior to the participating components.

Until recently, anticorrosion pigments such as chromates were generally added to organic coatings to enhance longevity and to obstruct corrosion activity in the defect region [6,7]. However, most of these commercially available corrosion inhibitors are carcinogenic. Further, direct inclusion of an inhibitor into an organic coating can destabilize the film structure, thereby deteriorating its barrier properties. Thus, the development of minimally hazardous, high-performance protective coatings has now become a new area of exploration. Of late, a new strategy has been adopted to develop high-performance coatings by the intercalation or encapsulation of inhibitors in smart host/carriers with the triggered release of those ions on demand [8–11]. The idea behind using encapsulated inhibitors in a host system is for it to not only act as a physical barrier against corrosive entities but for it to also be a self-healing agent. In this respect, layered double hydroxide (LDH), the inorganic reservoir, has gained significant attention probably due to its high ion-exchange capacity and layered structure. Various anions of different sizes and shapes can be inserted into the interlayer spacing of LDH, which offers the prospect of easy release and substitution of anions. Thus, inhibitor ions can be intercalated within lamellar LDH containers, which facilitates the trapping of corrosive ions. Moreover, LDH, being a layered material, when incorporated in an organic coating, has good barrier properties and also provides significant corrosion inhibition at the metal/coating interface due to the presence of various functional groups.

Zheludkevich et al. developed Mg–Al and Zn–Al–LDH with a divanadate anion coating for corrosion protection of 2024 aluminum alloy [12]. The incorporation of divanadate-doped Zn–Al–LDH on a commercial primer showed improved corrosion protection and the performance was found to be comparable to that of chromate-based coatings. Alibakhshi et al. synthesized a PO_4^{3-}-encapsulated Zn–Al–LDH nanocontainer, which significantly reduced the corrosion rate of mild steel by releasing PO_4^{3-} [13]. Zn–Al–PO_4^{3-}–LDH was also applied into a silane film, and further epoxy coatings were applied on the steel samples with or without silane. The electrochemical results revealed significantly improved corrosion protection for the Zn–Al–PO_4^{3-} incorporated silane film coating against Zn–Al–NO_3^-. Alibakhshi et al. synthesized nitrate-, molybdate-, and phosphate-encapsulated Zn–Al–LDH/silane hybrid (based on a mixture of tetraethyl orthosilicate (TEOS) and 3-aminopropyltriethoxysilane (APTES)) nanocomposite coatings on a mild steel substrate [14]. Electrochemical results revealed that the silane coating in the presence of phosphate exhibited superior corrosion protection as compared to the molybdate- and nitrate- incorporated Zn–Al–LDH/silane hybrid. After carefully contemplating the prior published studies, it was found that there are still possibilities to further engineer LDH nanocontainers for organic coatings. The degree of dispersion of LDH nanocontainers in a polymer matrix and the adhesion of the coating on metal substrates are crucial for protective performance. As the LDH structure hosts plenty of hydroxyl groups on the edges and surface, its surface properties can be altered by grafting an appropriate entity, such as silane. The grafting of silane not only improves the compatibility between LDH and the polymer matrix, it also strengthens the coating adhesion on the metal structure. Thus, encapsulation of inhibitors within the interlayer space and functionalization could be a potential approach to improve the protective performance of an LDH-incorporated epoxy coating.

In this present work, to form good adhesion between the LHD/epoxy coating and the metal substrate, and to improve the protective performance, an encapsulation modification technique has been proposed. The inorganic molybdate anion, which is an efficient corrosion inhibitor, was intercalated into the interlayer spacing of Mg–Al–LDH through an ion exchange process and,

further, APTES was used to functionalize the LDH surface. It was expected that MoO_4^{2-} would provide longevity for the epoxy coating. On the other hand, APTES would act as the bridge improving the chemical affinity and interfacial interaction between LDH and epoxy matrix. Further, silane modification was expected to augment the adhesion of the LDH/epoxy coating with the metal substrate.

2. Experimental

2.1. Materials

Bisphenol-A epoxy resin, with the trade name LAPOX*C-51, and cycloaliphatic amine hardener, with trade name LAPOX AH-428, were purchased from Atul Limited (Gujarat, India) for coating purposes. $Mg(NO_3)_2{\cdot}6H_2O$, $Al(NO_3)_3{\cdot}9H_2O$, and sodium molybdate (Na_2MoO_4) were purchased from Merck, India and were used as received. Tetrahydrofuran (THF) was purchased from SRL, Mumbai, India. APTES was purchased from Sigma Aldrich (St. Louis, MO, USA). The mild steel (Fe10W) substrate was purchased from a local market in Durgapur, India.

2.2. Preparation of MgAl–NO_3^-–LDH and MoO_4^{2-}-Intercalated MgAl–NO_3^-–LDH

MgAl–NO_3^-–LDH was synthesized by a co-precipitation method. In brief, $Mg(NO_3)_2{\cdot}6H_2O$ (0.025 mol, 19.65 g) and $Al(NO_3)_3{\cdot}9H_2O$ (0.075mol, 9.25 g) salt with an Mg/Al ratio of 3 was dissolved completely in 100 mL of distilled water. The mixed solution was taken in a burette and added drop wise to another solution containing 0.25 mol (2.124 g) $NaNO_3$ and 0.2 mol (8 g) NaOH while stirring. The pH of the solution was kept at ~10 by using 1M NaOH solution. The white precipitate so formed was left to age at 70–75 °C for 16h.After cooling to room temperature, the precipitate was filtered by repeatedly washing with deionized water till the pH reached 7 and then dried at 80 °C for 24 h inside a vacuum oven. For MoO_4^{2-} intercalation, first, ~2.5 g of MgAl–NO_3^-–LDH was ground into a fine powder; then, the powder was suspended in 100 mL of distilled water containing ~1.2 g $Na_2MoO_4{\cdot}2H_2O$. The suspended solution was vigorously stirred at 70 °C for 12 h and then further refluxed for another 6 h to obtain a white powder of MoO_4^{2-} intercalated LDH (Mo–LDH).

2.3. Preparation of APTES-Surface-Modified Mo–LDH

The functionalization of Mo–LDH was carried out according to our previous report [15]. In brief, finely powdered Mo–LDH was suspended in a mixture of distilled water (75 mL) and ethanol (25 mL) in a three-necked flask at ~50 °C for ~30 min under nitrogen atmosphere. About, 0.5 g of APTES was dissolved in the mixture of anhydrous ethanol (45 mL) and water (5 mL). The APTES solution was then added dropwise to the Mo–LDH suspension with constant stirring. Acetic acid was added till the pH reached ~3, after which the temperature was increased to 90 °C and left for ~24 h under nitrogen atmosphere. After cooling to room temperature, the white precipitate was filtered by washing with distilled water and ethanol and it was kept under vacuum at 80 °C for 24 h. The APTES-modified Mo–LDH was designated as APTES–Mo–LDH.

2.4. Preparation of APTES–Mo–LDH/Epoxy Coatings

For the preparation of the epoxy composite coating, ~150 mg (1 wt.% with respect to the epoxy hardener system) of APTES–Mo–LDH powder was dispersed in 100 mL of THF using bath sonication for 1 h. To that dispersion, ~10 g of epoxy resin (epoxy resin hardener ratio used in this present study was 2:1) was added to the APTES–Mo–LDH dispersion, and the suspension was further sonicated for 1 h. The solvent was evaporated by heating the suspension with constant stirring on a hot plate at ~70 °C for 5 h under reduced pressure. The APTES–Mo–LDH/epoxy suspension was placed inside a vacuum oven at ~70 °C for ~16 h for the complete removal of residual solvent. The APTES–Mo–LDH/epoxy suspension was cooled to ambient temperature and the weighed amount (5 g) of low-viscosity hardener was blended using high-speed laboratory mechanical mixture at

~1800 rpm for 4 min. The sticky suspension was then kept inside a degassing chamber for ~30 min to remove air bubbles. The mixture was then coated on a mild steel plate using a spin coater and cured at room temperature for 24 h. The coated steel substrate was placed inside vacuum desiccators for further characterization. Before coating the composite, the surfaces of the steel substrate were mechanically ground with SiC papers to achieve uniform smoothness and roughness and then cleaned ultrasonically in acetone.

2.5. Characterization

Fourier-transform infrared (FTIR) spectra were recorded with a Perkin Elmer RXI FTIR in the frequency range of 4000–400 cm^{-1}. X-ray diffraction (XRD) of LDH, Mo–LDH, and APTES–Mo–LDH was carried out with PANalytical (Model X pert PRO) at a scan rate of 0.106° s^{-1} in the 2θ range of 10°–60°. Thermogravimetric analysis (TGA) was carried out with a Jupiter STA 449 F1, Netzsch, Germany to study the thermal degradation behavior of APTES–Mo–LDH. The samples (~5.56 mg) were heated from 30 to 750 °C at a heating rate of 5 °C min^{-1} under air atmosphere. Atomic force microscopy (AFM) of the coating sample was obtained on a Witec alpha300 R. Field emission scanning electron microscopy (FE-SEM) was carried out with a ∑igma HD, Carl Zeiss, Germany. The inhibition performances of the APTES–Mo–LDH/epoxy coating were studied by using electrochemical impedance spectroscopy (EIS) and polarization tests in 3.5% NaCl solution. An electrochemistry workstation (PARSTAT 4000, Princeton Applied Research) was used to perform potentiodynamic polarization curves and EIS. The electrochemical measurements were performed at 28 °C using a three-electrode configuration, where APTES–Mo–LDH/epoxy coated steel with an exposed area of 1 cm^2 was used as the working electrode (WE), platinum foil as counter electrodes (CEs), and a silver/silver chloride electrode (Ag/AgCl) as the reference electrode (RE). The measurements were carried out using a double-jacketed corrosion cell covered with a Teflon plate containing drilled holes for the immersion of the electrodes. The test specimens were immersed in the 3.5 wt.% NaCl solution for 3 h before the electrochemical tests, allowing the specimen to stabilize. EIS measurements were carried out using a 10-mV amplitude sinusoidal signal at open circuit potential (OCP) in the frequency range of 10 kHz to 10 mHz. The inhibition efficiency (η) was calculated with the parameters derived from EIS measurement following this equation:

$$\eta\ (\%) = \frac{R_{ct} - {R_{ct}}^o}{R_{ct}} \times 100 \quad (1)$$

where ${R_{ct}}^o$ and R_{ct} are the charge transfer resistance of blank and APTES–Mo–LDH-coated samples, respectively, in 3.5% NaCl solution.

The potentiodynamic polarization test was performed after the EIS performance at a scan rate of 0.5 mV/s from −250 to 250 mV. The two crucial parameters—corrosion potential (E_{corr}) and corrosion current (I_{corr})—were extracted from the polarization curve, which were then used to quantify the corrosion protection efficiency, *PE* (%), following this equation:

$$PE\ (\%) = \frac{{I_{corr}}^o - I_{corr}}{{I_{corr}}^o} \times 100 \quad (2)$$

where ${I_{corr}}^o$ and I_{corr} are the corrosion current density of blank and APTES–Mo–LDH-coated samples, respectively, in 3.5% NaCl solution. The corrosion rate, R_{corr}, in milli-inches per year (MPY), was calculated according to the following formula [16]:

$$R_{corr}(MPY) = \frac{I_{corr} \cdot K \cdot EW}{\rho A} \quad (3)$$

where K is a constant, thevalue of which was 1.288 × 105 milli-inches/(amp-cm-year); EW is the equivalent weight of the sample; ρ is the density (g/cm^3) of the sample; and A is the exposed surface area (cm^2) of the sample.

3. Results and Discussion

3.1. Characterization of LDH, Mo–LDH, and APTES–Mo–LDH

Figure 1 shows the schematic of intercalation and modification of LDH and the probable interaction with the epoxy matrix. FTIR and XRD were used to trace the chemical composition and phase of the prepared LDH. Figure 2a depicts the IR spectra of MgAl–NO_3–LDH, Mo–LDH (MgAl–MoO_4–LDH), and APTES–Mo–LDH. The intense band observed at 1384 cm^{-1} is ascribed to the stretching mode of NO_3^- anions, which confirmed the presence of nitrate ions in the interlayer of MgAl–LDH [17]. The band at ~1640 cm^{-1} can be attributed to the bending vibration of -OH and interlayer crystal water. Further, the bands observed at the lower region of 500–800 cm^{-1} could be assigned to the lattice vibration modes of O–M–O and M–O (M = Mg, Al) [18]. The absorption band at ~890 cm^{-1} in the spectra of MgAl–MoO_4–LDH (Figure 2a) is indexed to the presence of molybdate anions in the LDH interlayer [19]. The FTIR spectrum of APTES–MgAl–MoO_4–LDH was found to be different from that of pristine LDH and MoO_4-intercalated LDH. The intense peaks at 1579 and 1475 cm^{-1} could be ascribed to the -NH_2 scissoring of the grafted APTES. The intense peak at 983 cm^{-1} is assigned to the Si–O–M vibration, which confirmed the grafting of APTES molecules on molybdate-intercalated LDH the through the condensation reaction between Si–OH and –OH of the LDH layers [20]. The presence of a peak at 983 cm^{-1} in APTES-grafted LDH further confirmed the molybdate intercalation.

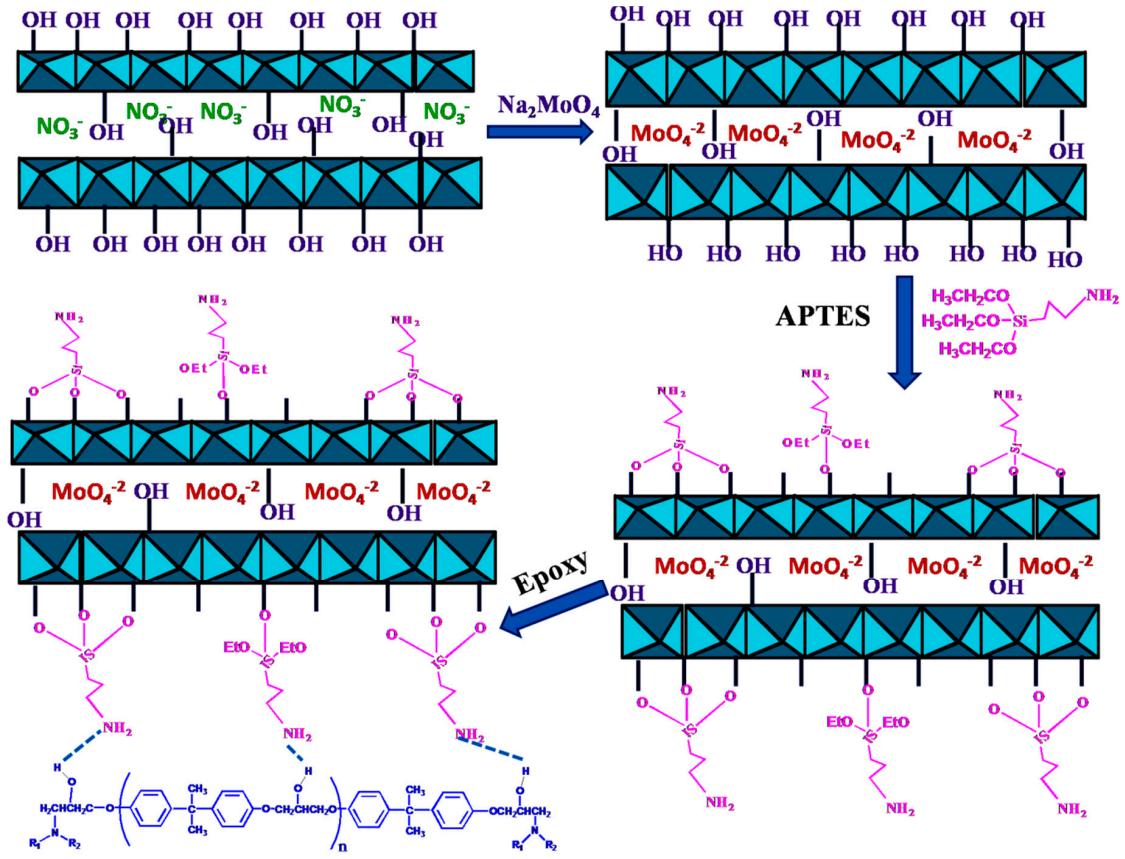

Figure 1. Schematic for the intercalation and modification of layered double hydroxide (LDH) and the possible interaction with the epoxy matrix.

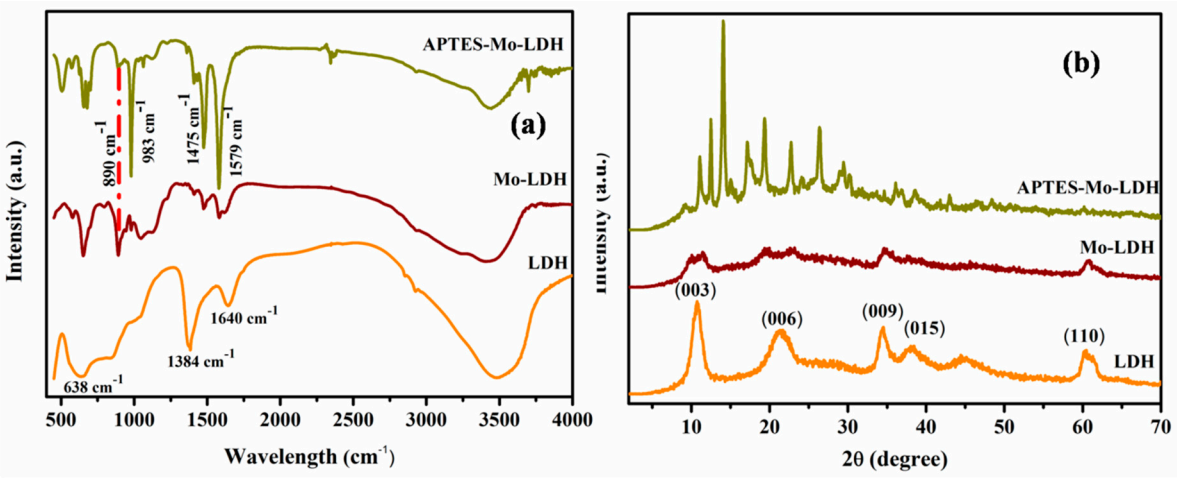

Figure 2. (**a**) Fourier-transform infrared (FTIR) spectra and (**b**) X-ray diffraction (XRD) pattern of LDH, Mo–LDH, and 3-aminopropyltriethoxysilane(APTES)–Mo–LDH.

Figure 2b shows the XRD patterns of MgAl–NO_3–LDH, Mo–LDH, and APTES–Mo–LDH in the 2θ range of 2°−70°. The diffraction peak of MgAl–NO_3–LDH with 2θ = 10.7°, 21.3°, 34.5°, and 38.2° corresponding to the (003), (006), (009), and (015) reflections indicated the characteristic hydrotalcite structure [21]. After intercalation of molybdate anions, a slight displacement of diffraction peaks towards low 2θ angle was observed. However, the basal spacings were not affected significantly, which might be due to the small number of molybdate anions or the possibility that molybdate ions assumed some unusual structure within the LDH interlayer. It can be seen from the diffraction of Mo–LDH that the intensity of all peaks diminished after molybdate exchange, which indicated that the crystallinity was hampered in the presence of molybdate anions in comparison with nitrate ions. The XRD of APTES–Mo–LDH exhibited all the peaks characteristic of a hydrotalcite structure. Grafting of silane did not significantly alter the spacing of LDH, which suggested that the surface hydroxyl of hydrotalcite reacted with silane. However, reflections of APTES–Mo–LDH were found to intensify, which suggested that the grafting of silane onto the surface hydroxyl groups of LDH had little influence on the long-range order of LDH during the modification procedure [22].

In order to corroborate the content of nitrate, molybdate, and other volatile materials, MgAl–NO_3–LDH and its derivatives (Mo–LDH and APTES–Mo–LDH) were subjected to thermal degradation in an air atmosphere from room temperature to 750 °C. Figure 3a,b shows the TGA thermograms of LDH, Mo–LDH, and APTES–Mo–LDH. Thermal analyses of pristine MgAl–NO_3–LDH showed a two-step weight loss, the first step (I) from 30 to 220 °C with a total mass loss of ~11.29%. The weight loss at this temperature is ascribed to the elimination of physisorbed water molecules, those intercalated water molecules on the LDH interlayer gallery, and nitrate ions present in LDH surface. The second thermal degradation (II)started from ~220 °C and ended at ~555 °C, which is attributed to the dehydroxylation of metal hydroxide and the removal of nitrate ions to form mixed metal oxides. The Mo–LDH also showed two-step degradation behaviors, the first step beginning at 30 °C and ending at 242 °C. The weight loss at this range was due to the removal of absorbed water and the dehydroxylation of double hydroxide. The second step, starting from 242 °C and ending at 510 °C, is ascribed to the transformation of molybdate into molybdenum oxide. The APTES-grafted Mo–LDH (APTES–Mo–LDH) showed a thermal degradation trend quite different from that of pristine LDH and Mo–LDH (Figure 3b). The mass loss peak corresponding to the absorbed water molecules disappeared completely, indicating water consumption during the grafting of APTES with LDH. Further, the difference in weight loss corresponding to dehydroxylation was found to be narrowed as compared with unmodified LDH and Mo–LDH. The reduced content of -OH groups confirmed their consumption during the condensation reaction with -Si–OH to form -Si–O–M. The weight loss within the range of 388–600°C was indexed to the decomposition of the alkyl chain and the loss of

OH and SO_2 from the surface and the formation of spinels. The thermal decomposition behavior of APTES–Mo–LDH was well substantiated with FTIR peaks, confirming the grafting of the APTES moiety on the LDH surface.

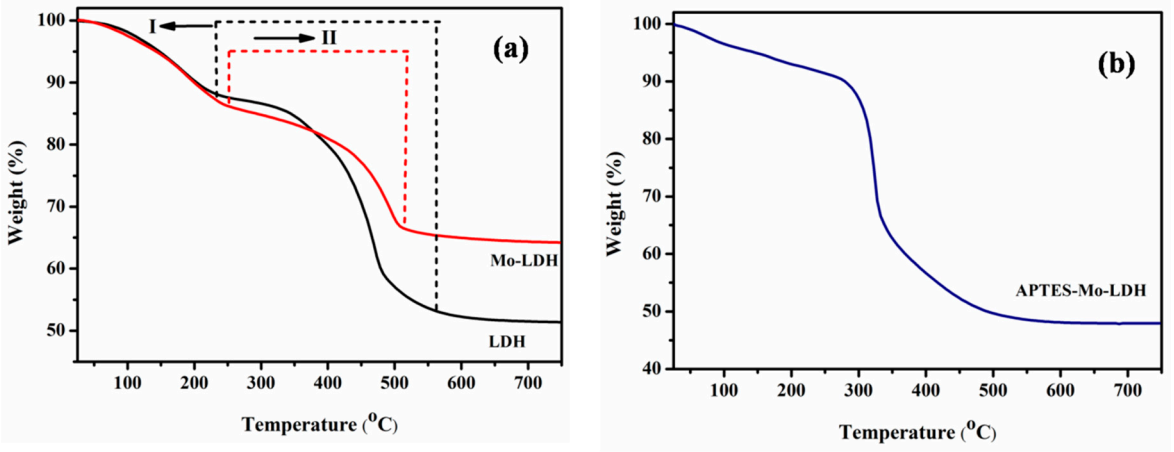

Figure 3. (**a**,**b**) Thermogravimetric analysis (TGA) thermogram of LDH, Mo–LDH, and APTES–Mo–LDH.

3.2. FE-SEM Analysis of Coatings

To illustrate the influence of the functionalized LDH/epoxy composite coating on anticorrosion performance, the surface analysis of the coated samples was studied after immersion in a corrosive environment. The FE-SEM morphologies of the bare steel, epoxy coating, and composite coating after 12 h of immersion are shown in Figure 4a–d. As evident from Figure 4a, the rough degraded surface of the bare steel indicated the initiation of the corrosion process. The compact smooth layer of the epoxy coating (Figure 4b) did not show any accumulated corrosion products, which indicated that the corrosion was delayed as compared with the bare steel.

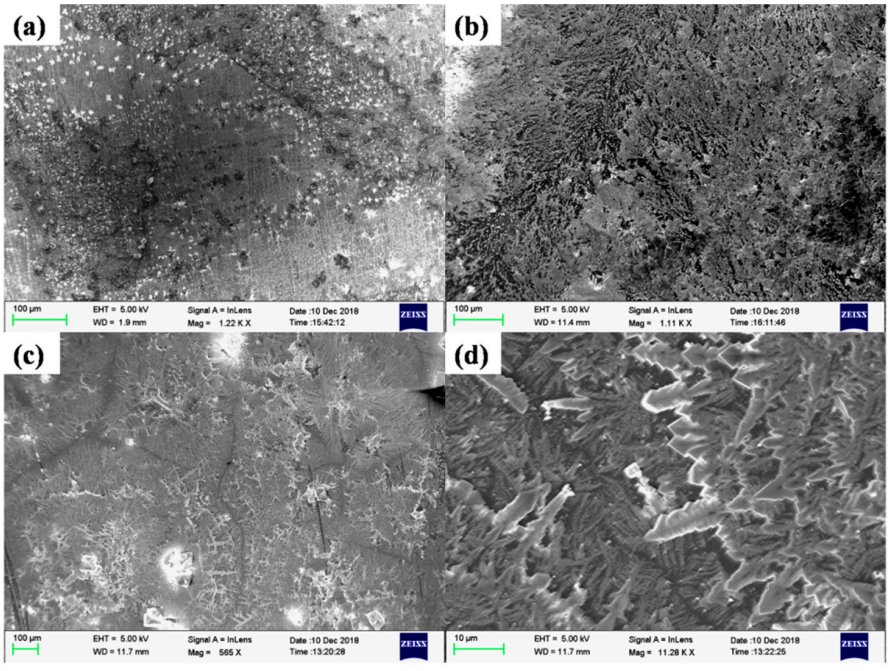

Figure 4. The field emission scanning electron microscopy(FE-SEM) micrographs of the (**a**) bare steel surface, (**b**) epoxy coating, and (**c**,**d**) low and high magnification of the composite coating after exposure to3.5 wt.% NaCl for 12 h.

On the other hand, the composite-coated sample (Figure 4c) showed dendritic-like morphology. A continuous smooth serrated edge of the coating appeared to cover the steel substrate without any ripples and deposited corrosion product. The higher magnification morphology of the composite coating, as shown in Figure 4d, revealed uniform vertically grown coating on the substrate. It was interesting to note that the morphology of the composite coating was found to be smoother and more uniform than the pure epoxy coating. The smooth and compact surface of the composite coating indicated that the functionalized LDH was able to improve the adherence of the coating over the metal surface. The distinctive morphology of the composite coating without any palpable voids and deposited corrosion products indicates the efficient anticorrosion ability of APTES–Mo–LDH. To calculate the probable coating thickness, AFM of the composite coating was performed. Figure 5a–c shows the surface topography of the composite coating and the corresponding 3-D image. The coating region of the surface appeared smooth, while the uncoated surface seemed rough. The thickness of the coating was calculated to be ~255 nm.

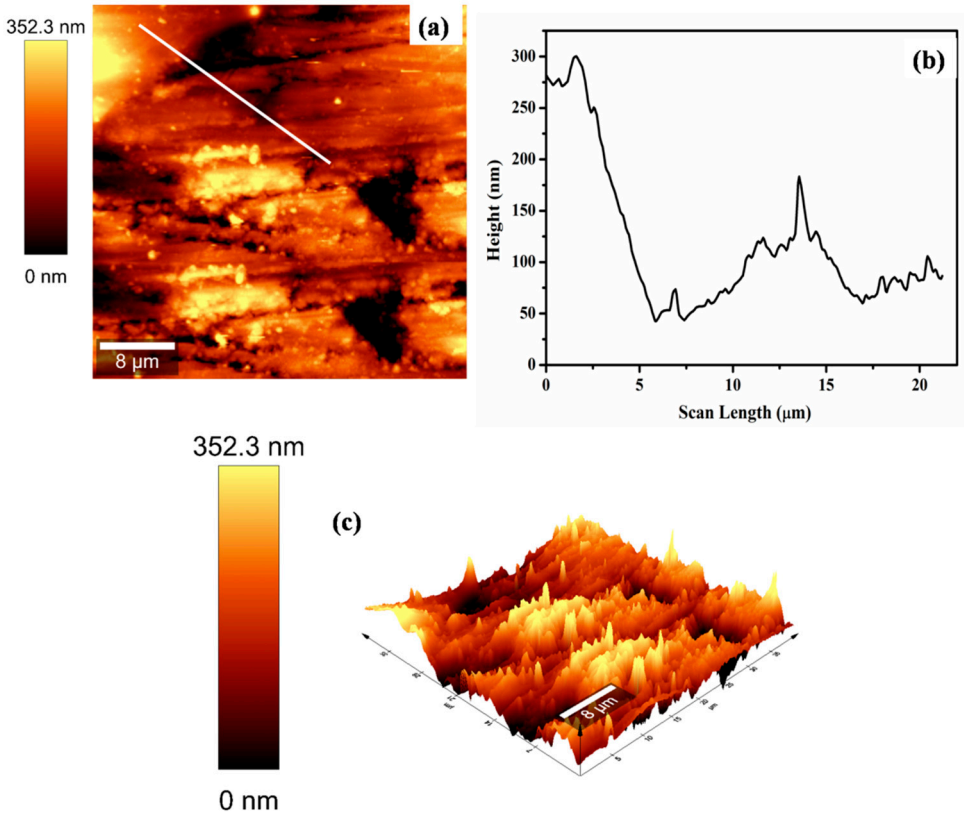

Figure 5. (**a**,**b**) Atomic force microscopy (AFM) topography and cross-sectional profile of composite coating and (**c**) 3-D image of corresponding topography.

3.3. Impedance Measurements and Potentiodynamic Polarization Analysis

Electrochemical impedance spectroscopy (EIS) was performed at the OCP to comprehend the corrosion resistance provided by pure epoxy and the epoxy composite coating containing 1 wt.% of APTES–Mo–LDH. Figure 6a–d depicts the impedance diagrams achieved after exposure for 3 h in 3.5% NaCl solution. The radius of the impedance curvature, as seen from the Nyquist plot (Figure 6b) of the composite coating, was found to be higher than the epoxy coating, which indicated larger Faradaic resistance to the corrosion process. The dimension of the radius of impedance corresponded to the extent of resistance imposed by the coating on the charge transfer process. The small impedance arc of the epoxy coating, compared with the composite coating, suggested that the corrosive ions passed through the coating with less hindrance, thus, the higher corrosion rate. The APTES–Mo–LDH composite coating resulted in higher Faradaic resistance, making the corrosion process more sluggish.

The augmented inhibition performance of APTES–Mo–LDH epoxy composites was ascribed to the formation of boundary film on the metal substrate and the release of molybdate anions from the LDH interlayer galleries, making room for corrosive Cl^-. Thus, the composite coating displayed superior corrosion protection. The obtained electrochemical results confirmed that APTES–Mo–LDH was able to provide excellent protection for the steel substrate.

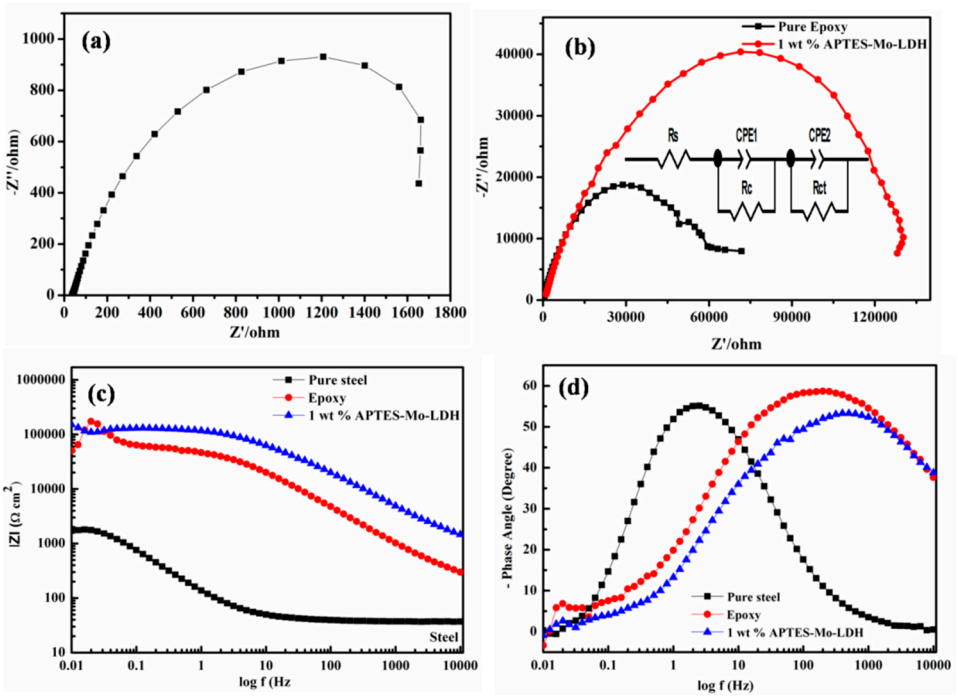

Figure 6. (**a**,**b**) Electrochemical impedance spectroscopy (EIS) plots of bare steel, epoxy coating, and composite coating. (**c**,**d**) Bode plots of bare steel, epoxy coating, and composite coating.

Generally, magnitude of impedance moduli, Z, at low frequencies ($|Z|_{0.01Hz}$) is used to quantify resistance to corrosion rendered by the coating, and higher $|Z|_{0.01\ Hz}$ suggest superior corrosion resistance [23,24]. The epoxy composite coating containing 1 wt.% of APTES–Mo–LDH (Figure 6c) showed a Z value of $1.5 \times 10^5\ \Omega{\cdot}cm^2$, which far exceeded the epoxy coating value of $4.9 \times 10^4\ \Omega{\cdot}cm^2$. The magnitude of Z values at 0.01 Hz for the composite and epoxy coatings exhibited the same trend as that of Faradaic resistance. The highest impedance magnitude of the epoxy composite coating at a low frequency suggested that this coating rendered excellent inhibition properties. Therefore, APTES–Mo–LDH can effectively impede the diffusion of corrosive ions to the metal interface, thus diminishing the corrosion rate of the steel substrate. Further, the improved resistance to the corrosion process could also be due to the presence of silane groups on the LDH surface that might have firmly adhered to the substrate, inhibiting the dissolution of the metal. Figure 6d represents Bode plots of the bare steel, epoxy-coated, and composite-coated substrate after immersion for 3 h. The Bode phase angle plots for the composite coating exhibited two time constants, which is attributed to the coating response and the redox reaction, respectively. The time constants for epoxy and composite coating shifted towards a higher frequency, which indicated that the metal surface was well protected. In other words, it signifies that the formation of boundary layers acted as a barrier and prevented the corrosive ions from being diffused. The equivalent electrical circuit corresponding to two time constant spectra were proposed to model the investigated system, which is depicted in Figure 6b (insert), where R_s is the solution resistance, Rc characterizes the coating resistance, R_{ct} represents charge transfer resistance, and CPE1 and CPE2 represent the coating and double layer capacitance, respectively [25,26]. The derived electrochemical parameters are summarized in the Table 1. Generally, the magnitude of R_c was used to evaluate the extent of anticorrosion performance of composites

coating. The R_c of the composite coating was found to be 62,000 Ω·cm^2, which was significantly higher than the epoxy coating value of 54,000 Ω·cm^2. Further, the composite coating showed a lower coating capacitance value, which could be attributed to the diminished diffusion of corrosive ions in the presence of APTES–Mo–LDH.

Table 1. Electrochemical parameters derived from the impedance plot.

Sample Type	R_s (Ω·cm^2)	CPE1 (mF·cm^{-2})	R_c (Ω·cm^2)	CPE2 (mF·cm^{-2})	R_{ct} (Ω·cm^2)	η %
Steel	37.25	0.000496	900	0.000411	290	-
Epoxy coating	162.5	9.39×10^{-7}	54,000	0.032	32,000	-
Composite coating	1000	1.9×10^{-7}	62,000	7.19×10^{-7}	72,000	99

The polarization performance of the epoxy and composite coatings were scanned from cathodic to anodic regions to analyze the corrosion protection properties. Figure 7 represents the potentiodynamic polarization curves of pure steel, epoxy-coated, and composite-coated steel in 3.5 wt.% NaCl aqueous solution. As expected, pure steel showed the most negative corrosion potential (E_{corr}) value. It was found that after coating the steel surface with epoxy, the E_{corr} was found to shift towards the positive direction against pure steel. In order to quantitatively extract the crucial parameters, such as E_{corr}, current density (I_{corr}), and protection efficiency (PE) [27,28], the polarization curves were extrapolated and the values are summarized in Table 2. The corrosion resistance competency of the coating can be computed from the magnitude of the E_{corr} and I_{corr}. Usually, higher E_{corr} and lower I_{corr} values characterize the extent of the corrosion resistance effectiveness of the coating material. The E_{corr} of the composite coating containing 1wt.% of APTES–Mo–LDH was found to be −381.84 mV, while that of the epoxy coating was −531.443 mV. The significant positive shift in the E_{corr} value of the composite coating and the higher cathodic (β_c) and anodic (β_a) Tafel slope could be correlated to the cathodic and anodic inhibition mechanism. The I_{corr} value of the composite coating was found to be 2.9×10^{-5} μa/cm^2,which was significantly lower than the epoxy coating (3.9×10^{-4} μa/cm^2). The significant decrease in current density was ascribed to the inhibitive barrier formed by the molybdate-intercalated LDH on the steel surface, barricading the anodic and cathodic sites and impeding corrosive ion ingress to the metal surface. In summary, the analysis of E_{corr} and I_{corr} indicated that APTES–Mo–LDH remarkably impeded the diffusion of corrosive ions to the interface and thus prevented the dissolution of the metal. The corrosion rate (R_{corr}) of the composite coating was found to decrease by ~98%, which proved the superior performance of APTES–Mo–LDH as an anticorrosion material.

Table 2. Corrosion potential (E_{corr}), corrosion current density (I_{corr}), corrosion protection efficiency (PE), and corrosion rate (R_{Corr}) derived from Tafel plot extrapolation.

Sample Type	E_{Corr} versus Ag/AgCl (mV)	I_{Corr} (μa/m^2)	β_a (mV·dec^{-1})	β_c (mV·dec^{-1})	PE (%)	R_{Corr} (MPY)
Steel	−718.689	0.002	42.1	85.0	-	611.55
Epoxy coating	−531.443	0.000 396	43.0	102.0	80.2	121.00
Composite coating	−381.843	0.000 029	53.1	139.1	98.5	8.86

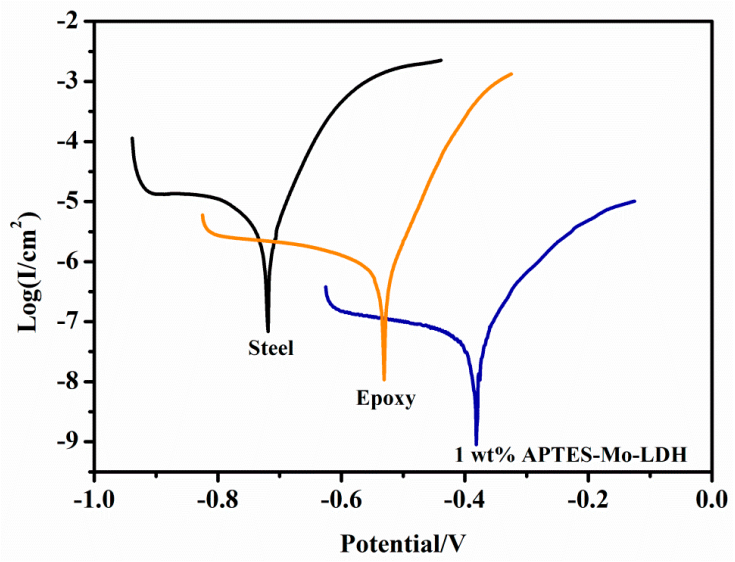

Figure 7. Tafel plot of bare steel, epoxy coating, and composite coating.

3.4. Inhibition Mechanism of the Composite Coating

It has been proposed that the formation of surface oxide is crucial for the corrosion inhibition of a metal substrate by molybdate anions [29,30]. It is anticipated that the MoO_4^{2-} anion would be adsorbed onto the oxide surface through hydrogen bonding between molybdate oxygen atoms and hydrogen atoms of hydroxyl groups of surface oxide, making the surface negatively charged. The negatively charged MoO_4^{2-}-adsorbed surface would repeal the corrosive ions, thereby disturbing the interaction between the metal surface and corrosive ions. The MoO_4^{2-}-anion-intercalated LDH coating showed superior corrosion resistance because the prospect of ion exchange protected the layered structure from being decomposed in the presence of Cl^- ions. The augmented corrosion performance can be ascribed to the absorption of Cl- ions within the galleries of LDH and the release of MoO_4^{2-} anions, as depicted in Equation (3). Further, MoO_4^{2-} anions also had the tendency to react with Fe^{+2} [31], according to Equation (4):

$$\text{LDH-}MoO_4^{2-} + 2Cl^- \rightarrow \text{LDH-}2Cl^- + MoO_4^{2-} \quad (4)$$

$$Fe^{+2} + MoO_4^{2-} \rightarrow [Fe^{+2} \ldots \ldots MoO_4^{2-}] \quad (5)$$

As per the reaction pertaining to Equations (1) and (2), the released MoO_4^{2-} anions formed a diffusion layer on the coating surface, which acted as an effective inhibitor to protect the metal substrate from dissolution. The presence of MoO_4^{2-} in the boundary layer largely impeded the absorption of Cl^- ions. Thus, the ion exchange facility of LDH and the inhibiting activity of MoO_4^{2-} anions led to the improved corrosion resistance of the coating. On the basis of these two mechanisms, namely, ion exchange and competitive adsorption of ions, the inhibition mechanism is proposed and is depicted in Figure 8.

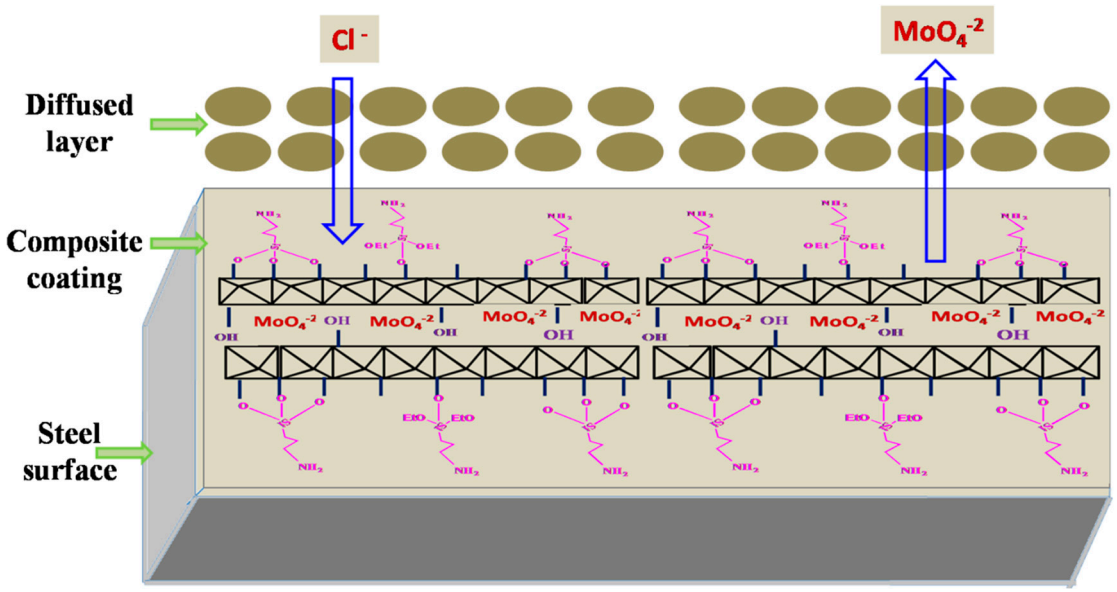

Figure 8. Schematic for the mechanism of corrosion inhibition by APTES–Mo–LDH/epoxy composite coating.

4. Conclusions

In summary, molybdate-anion-intercalated, functionalized Mg–Al–LDH was used to reinforce an epoxy polymeric coating for anticorrosion application. Molybdate anions were intercalated to exploit its corrosion inhibition properties and the surface was engineered to improve the interfacial interaction with the epoxy matrix and to firmly adhere the coating onto the steel substrate. The anticorrosion performance of the composite coating was evaluated using potentiodynamic polarization and electrochemical impedance spectroscopy techniques. To further understand the corrosion process at the interface, the impendence data was fitted using an equivalent electrical circuit. The electrochemical results revealed improved anticorrosion performance of the composite coating, on the basis of which the probable inhibition mechanism was proposed. At 1 wt.% APTES–Mo–LDH, the composite coating showed more than 98% protection efficiency. The corrosion rate of the composite coating calculated from potentiodynamic polarization results revealed a ~98% reduction compared with bare steel.

Author Contributions: T.K. designed and coordinated the research work, S.C. performed all the experiments, N.C.M. helped in analyzing the data, and all the authors assisted the assembly and editing of the manuscript.

Funding: This research was funded by the Department of Science and Technology, New Delhi, India (GAP211412).

Acknowledgments: Authors are thankful to the Director of Council of Scientific and Industrial Research-Central Mechanical Engineering Research Institute.

Conflicts of Interest: The authors declare no conflict of interest.

References

1. Xu, B.; Gong, W.; Zhang, K.; Yang, W.; Liu, Y.; Yin, X. Theoretical prediction and experimental study of 1-Butyl-2-(4-methylphenyl)benzimidazole as a novel corrosion inhibitor for mild steel in hydrochloric acid. *J. Taiwan. Inst. Chem. Eng.* **2015**, *51*, 193–200. [CrossRef]
2. Rahman, O.; Ahmad, S. Physico-mechanical and electrochemical corrosion behavior of soy alkyd/Fe_3O_4 nanocomposite coatings. *RSC Adv.* **2014**, *4*, 14936–14947. [CrossRef]
3. Abdollahi, H.; Ershad-Langroudi, A.; Salimi, A.; Rahimi, A. Anticorrosive Coatings prepared using Epoxy-Silica Hybrid Nanocomposite Materials. *Ind. Eng. Chem. Res.* **2014**, *53*, 10858–10869. [CrossRef]
4. Ji, W.G.; Hu, J.M.; Zhang, J.Q.; Cao, C.N. Reducing the water absorption in epoxy coatings by silane monomer incorporation. *Corros. Sci.* **2006**, *48*, 3731–3739. [CrossRef]

5. Ramezanzadeh, B.; Attar, M.M. Studying the corrosion resistance and hydrolytic degradation of an epoxy coating containing ZnO nanoparticles. *Mater. Chem. Phys.* **2011**, *130*, 1208–1219. [CrossRef]
6. Raps, D.; Hack, T.; Wehr, J.; Zheludkevich, M.L.; Bastos, A.C.; Ferreira, M.G.S.; Nuyken, O. Electrochemical study of inhibitor-containing organic–inorganic hybrid coatings on AA2024. *Corros. Sci.* **2009**, *51*, 1012–1021. [CrossRef]
7. Blustein, G.; Di Sarli, A.R.; Jaén, J.A.; Romagnoli, R.; Del Amo, B. Study of iron benzoate as a novel steel corrosion inhibitor pigment for protective paint films. *Corros. Sci.* **2007**, *49*, 4202–4231. [CrossRef]
8. Williams, G.; McMurray, H.N. Anion-Exchange Inhibition of Filiform Corrosion on Organic Coated AA2024-T3 Aluminum Alloy by Hydrotalcite-Like Pigments. *Electrochem. Solid-State Lett.* **2003**, *6*, B9–B11. [CrossRef]
9. Buchheit, R.G.; Guan, H.; Mahajanam, S.; Wong, F. Active Corrosion Protection and Corrosion Sensing in Chromate-Free Organic Coatings. *Prog. Org. Coat.* **2003**, *47*, 174–182. [CrossRef]
10. Stimpfling, T.; Leroux, F.; Hintze-Bruening, H. Organo-Modified Layered Double Hydroxide in Coating Formulation to Protect AA2024 from Corrosion. *Colloids Surf. A* **2014**, *458*, 147–154. [CrossRef]
11. Poznyak, S.K.; Tedim, J.; Rodrigues, L.M.; Salak, A.N.; Zheludkevich, M.L.; Dick, L.F.P.; Ferreira, M.G.S. Novel Inorganic Host Layered Double Hydroxides Intercalated with Guest Organic Inhibitors for Anticorrosion Applications. *ACS Appl. Mater. Interfaces* **2009**, *1*, 2353–2362. [CrossRef] [PubMed]
12. Zheludkevich, M.L.; Poznyak, S.K.; Rodrigues, L.M.; Raps, D.; Hack, T.; Dick, L.F.; Nunes, T.; Ferreira, M.G.S. Active protection coatings with layered double hydroxide nanocontainers of corrosion inhibitor. *Corros. Sci.* **2010**, *52*, 602–611. [CrossRef]
13. Alibakhshi, E.; Ghasemi, E.; Mahdavian, M.; Ramezanzadeh, B.; Farashi, S. Fabrication and Characterization of PO_4^{3-} Intercalated Zn-Al-Layered Double Hydroxide Nanocontainer. *J. Electrochem. Soc.* **2016**, *163*, C495–C505. [CrossRef]
14. Alibakhshi, E.; Ghasemi, E.; Mahdavian, M.; Ramezanzadeh, B. Fabrication and characterization of layered double hydroxide/silane nanocomposite coatings for protection of mild steel. *J. Taiwan Inst. Chem. Eng.* **2017**, *80*, 924–934. [CrossRef]
15. Chhetri, S.; Adak, N.C.; Samanta, P.; Murmu, N.C.; Kuila, T. Rheological, Mechanical, and Thermal Properties of Silane Grafted Layered Double Hydroxide/Epoxy Composites. *Ind. Eng. Chem. Res.* **2018**, *57*, 8729–8739. [CrossRef]
16. Wessling, B. Passivation of metals by coating with polyaniline: Corrosion potential shift and morphological changes. *Adv. Mater.* **1994**, *6*, 226–228. [CrossRef]
17. Guo, X.X.; Xu, S.; Zhao, L.; Lu, W.; Zhang, F.; Evans, D.G.; Duan, X. One-step hydrothermal crystallization of a layered double hydroxide/alumina bilayer film on aluminum and its corrosion resistance properties. *Langmuir* **2009**, *25*, 9894–9897. [CrossRef]
18. Ding, P.; Qu, B. Synthesis and characterization of exfoliated polystyrene/ZnAl layered double hydroxide nanocomposite via emulsion polymerization. *J. Colloid Interface Sci.* **2005**, *291*, 13–18. [CrossRef]
19. Phuruangrat, A.; Thongtem, T.; Thongtem, S. Preparation, characterization and photoluminescence of nanocrystalline calcium molybdate. *J. Alloys Compd.* **2009**, *481*, 568–572. [CrossRef]
20. Tao, Q.; He, H.; Frost, R.L.; Yuan, P.; Zhu, J. Nanomaterials based upon silylated layered double hydroxides. *Appl. Clay Sci.* **2009**, *255*, 4334–4340. [CrossRef]
21. Kang, D.; Yu, X.; Tong, S.; Ge, M.; Zuo, J.; Cao, C.; Song, W. Performance and mechanism of Mg/Fe layered double hydroxides for fluoride and arsenate removal from aqueous solution. *Chem. Eng. J.* **2013**, *228*, 731–740. [CrossRef]
22. Tao, Q.; He, H.; Li, T.; Frost, R.L.; Zhang, D.; He, Z. Tailoring surface properties and structure of layered double hydroxides using silanes with different number of functional groups. *J. Solid State Chem.* **2014**, *213*, 176–181. [CrossRef]
23. Sun, W.; Wang, L.; Wu, T.; Pan, Y.; Liu, G. Synthesis of low-electrical-conductivity graphene/pernigraniline composites and their application in corrosion protection. *Carbon* **2014**, *79*, 605–614. [CrossRef]
24. Qian, M.; Soutar, A.M.; Tan, X.H.; Zeng, X.T.; Wijesinghe, S.L. Two-part epoxysiloxane hybrid corrosion protection coatings for carbon steel. *Thin Solid Films* **2009**, *517*, 5237–5242. [CrossRef]
25. Dai, N.; Zhang, L.C.; Zhang, J.; Chen, Q.; Wu, M. Corrosion behavior of selective laser melted Ti-6Al-4 V alloy in NaCl solution. *Corros. Sci.* **2016**, *102*, 484–489. [CrossRef]

26. Qin, P.; Liu, Y.; Sercombe, T.B.; Li, Y.; Zhang, C.; Cao, C.; Sun, H.; Zhang, L.C. Improved Corrosion Resistance on Selective Laser Melting Produced Ti-5Cu Alloy after Heat Treatment. *ACS Biomater. Sci. Eng.* **2018**, *4*, 2633–2642. [CrossRef]
27. Chen, Y.; Zhang, J.; Dai, N.; Qin, P.; Attar, H.; Zhang, L.C. Corrosion Behaviour of Selective Laser Melted Ti-TiBBiocomposite in Simulated Body Fluid. *Electrochem. Acta.* **2017**, *232*, 89–97. [CrossRef]
28. Bai, Y.; Gai, X.; Li, S.; Zhang, L.C.; Liu, Y.; Hao, Y.; Zhang, X.; Yang, R.; Gao, Y. Improved corrosion behaviour of electron beam melted Ti-6Al–4V alloy in phosphate buffered saline. *Corros. Sci.* **2017**, *123*, 289–296. [CrossRef]
29. Farr, J.P.G.; Seeney, A.M.; Bentley, A.J.; Earwaker, L.G. A technique for the in situ elemental analysis of electrode surfaces. *Surf. Technol.* **1984**, *23*, 99.
30. Farr, J.P.G.; Saremi, M.; Seeney, A.M.; Bentley, A.J.; Earwaker, L.G. Molybdates in aqueous corrosion inhibition—III. Effects of molybdate in the anodic filming of steel. *Polyhedron* **1986**, *5*, 547.
31. Mu, G.; Li, X.; Qu, Q.; Zhou, J. Molybdate and tungstate as corrosion inhibitors for cold rolling steel in hydrochloric acid solution. *Corros. Sci.* **2006**, *48*, 445–459. [CrossRef]